ISSN (Print) 1226-1750
ISSN (Online) 2233-6656
**Journal of Magnetics** 18(1), 57-64 (2013) http://dx.doi.org/10.4283/JMAG.2013.18.1.057

# Flux Linkage Estimation in a Switched Reluctance Motor Using a Simple Reluctance Circuit

**Cheewoo Lee***

*Department of Electrical Engineering, Kyungsung University, Busan 608-736, Korea*

(Received 5 January 2013, Received in final form 5 February 2013, Accepted 5 February 2013)

**Flux linkage of phase windings is a key parameter in determining the behavior of a switched reluctance motor (SRM) [1-8]. Therefore, the accurate prediction of flux linkage at aligned and unaligned rotor positions makes a significant contribution to the design of an SRM and its analytical approach is not straightforward due to nonlinear saturation in flux. Although several different approaches using a finite element analysis (FEA) or a curve-fitting tool have been employed to compute phase flux linkage [2-5], they are not suitable for a simple design procedure because the FEA necessitates a large amount of time in both modeling and solving with complexity for every motor design, and the curve-fitting requires the data of flux linkage from either an experimental test or an FEA simulation. In this paper, phase flux linkage at aligned and unaligned rotor positions is estimated by means of a reluctance network, and the proposed approach is analytically verified in terms of accuracy compared to FEA.**

**Keywords :** flux linkage, inductance, switched reluctance motor

## 1. Introduction

Variable speed brushless motors have been gaining significant attention in many applications requiring low cost, high performance, and easy manufacturability. Switched reluctance machines (SRMs) are strong candidates due to their inexpensive and simple magnetic configuration which has concentric windings on the stator poles and no windings or no permanent magnets on the rotor unlike other ac or permanent magnet machines [1]. SRMs are a better choice for high volume applications such as home appliances and power tools which are highly cost competitive. Due to relatively small number of phases, single and two-phase SRMs are more suitable for cost savings with regards to material in the motor and switching devices like IGBTs and diodes in the converter. Recently, a two-phase SRM comprising an E-core magnetic structure has been proposed due to its electromagnetic performance improvement [7], and in this paper, the E-core SRM is investigated in terms of its flux linkage since the motor has complex flux paths between eight stator and ten rotor poles compared to a conventional SRM such as four-stator-pole two-rotor-pole combination.

The rapid advance of personal computers has made FEA tools more attractive in the characterization of an electrical rotating machine, but a FEA model intensively requires numerical computation time. Another possible way to predict flux linkage is a curve-fitting tool, but the method requires the data of flux linkage from either an experimental test or an FEA simulation. Therefore, large computational burden in the FEA and a request for existing data in the curve-fitting do not easily allow those methods to be incorporated into iterative design studies. In this paper, phase flux linkage at aligned and unaligned rotor positions is estimated in a two-phase E-core SRM by means of a simple reluctance circuit, and the estimation of flux linkage in the proposed scheme is analytically verified in terms of accuracy compared to FEA.

## 2. E-core Structure and its Previous Analysis

Fig. 1(a) and 1(b) show the first E-core prototype and its core laminations, respectively. Due to the mechanical separation of the two E-shaped cores in the stator, their physical placement during manufacturing processes is an issue resulting in additional steps for better mechanical alignment when compared to a conventional SRM. In Fig. 1(b), the circular back iron in the stator results in a non-


*Corresponding author: Tel: +82-51-663-4696
Fax: +82-51-624-5980, e-mail: cwlee1014@ks.ac.kr

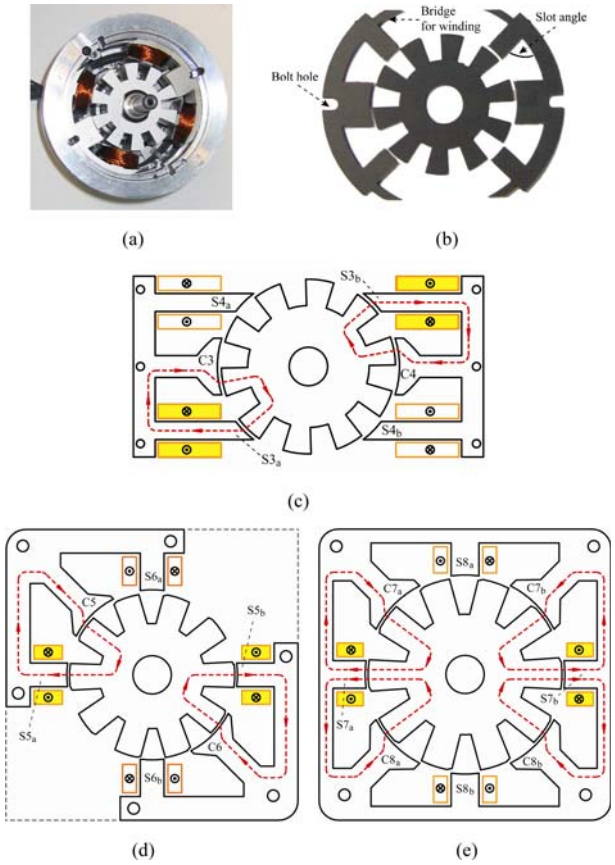


**Fig. 1.** (Color online) First E-core prototype and its design modifications, (a) Motor assembly, (b) Actual stator and rotor cores, (c) I-yoke segmented E-core SRM, (d) L-yoke segmented E-core SRM, (e) L-yoke single-body E-core SRM.

right-angular winding slot leading to some space loss for winding coils especially when adopting a fully automated direct winder or an indirect winding method using winding bobbins.

As shown in Fig. 1(c) and 1(d), two design modifications in the previous E-core magnetic structure incorporate a straight back iron in the stator segments to facilitate manufacturing. Their stator has two E-shaped stator cores where phase coils are concentrically wound on small poles (hereafter referred to as excitation poles) at the ends, and the two large common poles in between have no windings. This concept has two feasible implementations: an I-shaped yoke and an L-shaped yoke. In Fig. 1(e), there is another design modification where two more common poles are inserted in empty space of the L-yoke segmented E-core SRM, shown in Fig. 1(d). Among the given three design changes, the L-yoke single-body E-core SRM has been selected to be calculated in flux linkage since the structure consists of more complicated flux paths due to two more common poles compared to

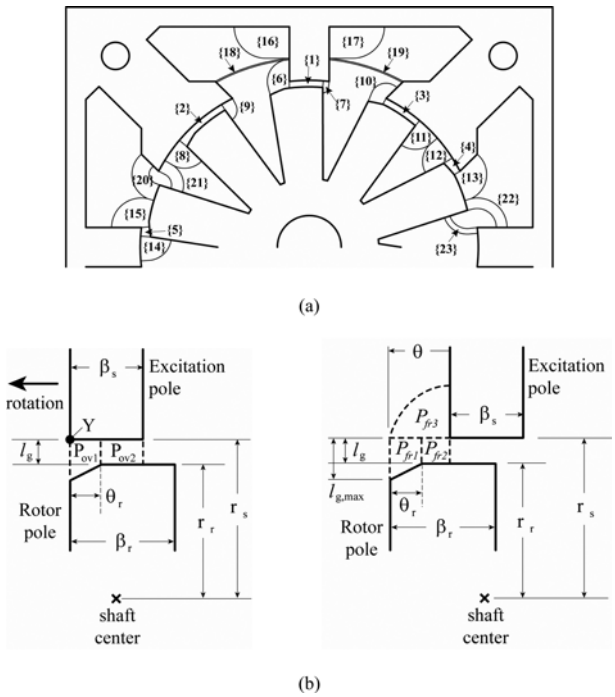


**Fig. 2.** Flux paths in air gap of L-yoke single-body E-core SRM, (a) Flux tubes representing permeances around air gap, (b) Zoomed-in overlap and fringing permeances.

the two segmented E-core SRMs.

Even though permeances in steel are inherently nonlinear because of magnetic saturation in B-H characteristics, the cross-sectional area and length of the corresponding flux paths are easy to calculate. However, as shown in Fig. 2(a), permeances in air gap are parametrically nonlinear because of the dimensional change on flux tubes with respect to rotor position. All the permeances in Fig. 2(a) are categorized into four types: overlap permeances in {1} to {5}, fringing permeances in {6} to {15}, slot leakage permeances in {16} to {19}, and pole-to-pole permeances in {20} to {23}, respectively [7]. The details of the overlap and fringing permeances are illustrated around an excitation pole as an example in Fig. 2(b). The overlap permeance is a summation of permeances $P_{ov1}$ and $P_{ov2}$, and the fringing permeance is a combination of permeances $P_{fr1}$, $P_{fr2}$, and $P_{fr3}$ given in Fig. 2(b). Using all the permeances representing each part of the L-yoke single-body E-core SRM as shown in Fig. 2, inductance estimation is conducted by magnetic equivalent circuit (MEC) technique, and for verifying the accuracy of the simulation, inductances from FEA and MEC are compared at 4A, 6A, and 8A as shown in Fig. 3. The maximum deviation between the FEA and MEC inductance is 9.2% and 3.8% at the unaligned and aligned rotor positions, respectively.

Although several different approaches using FEA or a

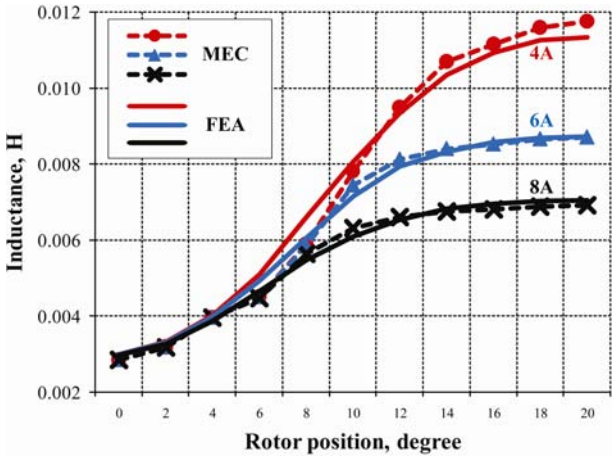


**Fig. 3.** (Color online) Inductance plots from MEC and FEA at various currents in L-yoke single-body E-core SRM.

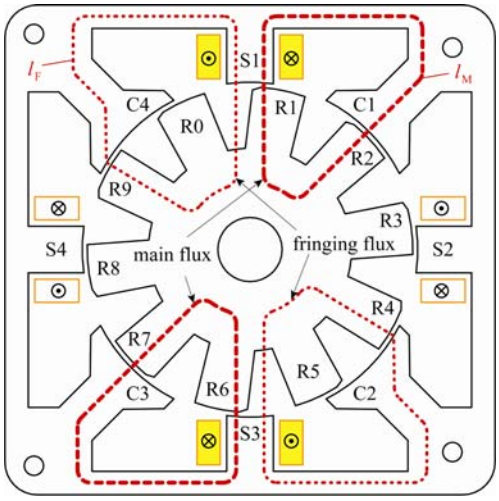


**Fig. 4.** (Color online) Main and fringing flux paths in two-phase single-body E-core SRM.

curve-fitting tool have been employed to compute phase flux linkage [2-5], they are not suitable for a simple design procedure because the FEA necessitates a large amount of time in both modeling and solving with complexity for every motor design, and the curve-fitting requires the data of flux linkage from either an experimental test or an FEA simulation. MEC technique becomes one of the candidates for predicting flux linkage, but it still requires a large amount of numerical derivation representing lots of permeances as shown in Fig. 2. Due to the complex permeance variation in the MEC, phase flux linkage at aligned and unaligned rotor positions is estimated by means of a simple reluctance circuit in this paper.

## 3. Flux Linkage Estimation using a Simple Reluctance Circuit

Flux linkage is dependent on current in phase windings and rotor position as well, and stator poles excited by concentric windings experience the variation of flux linkage between two rotor positions such as fully aligned and unaligned rotor positions. Therefore, flux linkage of phase windings is a critical factor in the performance of an SRM where there are more fringing paths in flux at unaligned rotor position. Since dimensional change in the flux paths is nonlinear, flux linkage at unaligned position is difficult to calculate with decent accuracy. In this paper, the estimation of flux linkage using a simple reluctance circuit is proposed, and the reluctance approach is analytically verified in terms of accuracy compared to FEA.

### 3.1. Investigation of flux paths

Two assumptions have to be made for the analytical calculation of flux linkage generated by phase windings. First, there is no leakage of the flux in air gap around stator and rotor poles. Second, as shown in Fig. 4, the total flux supplied by phase windings can be considered as a combination of main and fringing flux at a rotor position of partial overlap between stator excitation poles, S1 and S3, and rotor poles, R1 and R6, respectively. Flux circulation from the stator pole S1 is separated into two different paths one of which is main flux flowing through a closed loop $l_M$, and the other path for the fringing flux is represented by $l_F$ given in Fig. 4.

Using Ampere's circuital law along the paths $l_M$ and $l_F$, the sum of products of magnetic field intensity and the corresponding length in both steel and air gap around stator excitation (S1) and common poles (C1) in case of $l_M$ is equal to total MMF enclosed by each closed loop as expressed in (1) and (3).

$$H_{cm} \cdot l_{cm} + H_{gm1} \cdot l_{gm1} + H_{gm2} \cdot l_{gm2} = N_p \cdot I_p \tag{1}$$

where

$$l_{cm} = h_s + 2h_r + h_c + l_{sy} + l_{ry} \tag{2}$$

where $H_{cm}$, $H_{gm1}$, and $H_{gm2}$ in case of the main flux are magnetic field intensity in core and air gap around the stator pole S1 the common pole C1, respectively. $N_p$ and $I_p$ are the number of turns per pole and current flowing through the windings, respectively. $h_s$, $h_c$, and $h_r$ are pole height in excitation, common, and rotor poles, respectively. $l_{sy}$, $l_{ry}$ are flux path lengths in stator back iron and rotor back iron, respectively.

$$H_{cf} \cdot l_{cf} + H_{gf1} \cdot l_{gf1} + H_{gf2} \cdot l_{gf2} = N_p \cdot I_p \tag{3}$$

where

$$l_{cf} = h_s + h_r + h_c + l_{sy} + l_{ry} \tag{4}$$

where $H_{cf}$, $H_{gf1}$, and $H_{gf2}$ on the fringing path are magnetic field intensity in core and air gap around the stator pole S1 and the common pole C4, respectively.

### 3.2. Flux linkage estimation

Fig. 5 shows the reluctance network of the monolithic E-core SRM and illuminates the flow of flux regarding both the main and fringing flux paths. The two air-gap magnetic field intensities in (1) are expressed by each flux density as

$$H_{gm1} = \frac{B_{m1}}{\mu_0} \tag{5}$$

$$H_{gm2} = \frac{B_{m2}}{\mu_0} \tag{6}$$

Realizing that there are two more air-gap flux paths around non-excited stator poles, S2 and S4 in Fig. 4, two air-gap reluctances $\Re_{gm3}$ and $\Re_{fg3}$ around the non-excited stator poles are to be incorporated into the reluctance circuit given in Fig. 5. Another important understanding of the reluctance network is that the total flux $\phi_t$ is halved at the node X since the two air-gap reluctances of the non-excited stator poles are the same, and two other air-gap reluctances, $\Re_{gm2}$ and $\Re_{gf2}$, around common poles C1 and C4 are also considered to be the same due to the distinct design of the common-pole structure. As a result, air-gap flux density $B_{m2}$ of the common pole C1 is given in (7), from which the flux density is expressed as a combination of main and fringing flux as derived in (9).

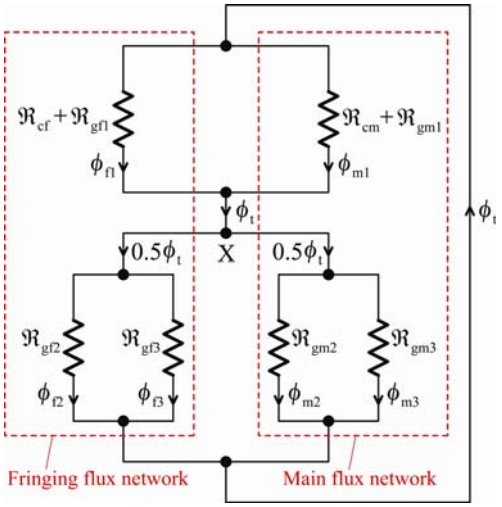


**Fig. 5.** (Color online) Reluctance network of single-body E-core SRM.

$$B_{m2} = \frac{\phi_{m2}}{A_{m2}} = \frac{0.5\phi_t}{A_{m2}} \frac{\Re_{gm3}}{\Re_{gm2} + \Re_{gm3}} \tag{7}$$

where

$$\frac{\Re_{gm3}}{\Re_{gm2} + \Re_{gm3}} = \frac{\dfrac{l_{gm3}}{\mu_0 A_{m3}}}{\dfrac{l_{gm2}}{\mu_0 A_{m2}} + \dfrac{l_{gm3}}{\mu_0 A_{m3}}} = \frac{l_{gm3} A_{m2}}{l_{gm2} A_{m3} + l_{gm3} A_{m2}} \tag{8}$$

$$B_{m2} = 0.5(\phi_{f1} + \phi_{m1}) \frac{l_{gm3}}{l_{gm2} A_{m3} + l_{gm3} A_{m2}} \tag{9}$$

By substituting (9) into (6), the air-gap magnetic field intensity around the common pole C1 is given by

$$H_{gm2} = \frac{\phi_{f1}}{\mu_0} C + \frac{\phi_{m1}}{\mu_0} C = \frac{\phi_{f1}}{\mu_0} C + \frac{A_{m1}}{\mu_0} C \cdot B_{m1} \tag{10}$$

where

$$C = \frac{0.5 l_{gm3}}{l_{gm2} A_{m3} + l_{gm3} A_{m2}} \tag{11}$$

Two magnetic field intensities, $H_{gm1}$ in (5) and $H_{gm2}$ in (10), are incorporated into (1), and hence,

$$H_{cm} \cdot l_{cm} = N_p I_p - \frac{C}{\mu_0} \phi_{f1} l_{gm2} - \frac{1}{\mu_0} (l_{gm1} + C \cdot A_{m1} l_{gm2}) B_{m1} \tag{12}$$

As the equation (1) has been converted to (6.44), regarding the fringing flux path, $l_F$, in Fig. 4, almost the same procedure can be applied as follows. It is straightforward to attain the analytical expression of air-gap flux density $B_{f2}$ around the common pole C4 as given in (17).

$$B_{f1} = \mu H_{cf} = \mu_0 H_{gf1} \tag{13}$$

$$H_{cf} = \frac{B_{f1}}{\mu} = \frac{\phi_{f1}}{\mu A_{f1}} \tag{14}$$

$$H_{gf1} = \frac{B_{f1}}{\mu_0} = \frac{\phi_{f1}}{\mu_0 A_{f1}} \tag{15}$$

$$B_{f2} = \frac{\phi_{f2}}{A_{f2}} = \frac{0.5\phi_t}{A_{f2}} \frac{\Re_{gf3}}{\Re_{gf2} + \Re_{gf3}} \tag{16}$$

$$B_{f2} = (\phi_{f1} + \phi_{m1}) D \tag{17}$$

where

$$D = \frac{0.5 l_{gf3}}{l_{gf2} A_{f3} + l_{gf3} A_{f2}} \tag{18}$$

By using (17), the corresponding air-gap magnetic field intensity is given by

$$H_{gf2} = \frac{B_{f2}}{\mu_0} = \frac{D}{\mu_0}(\phi_{f1} + \phi_{m1}) = \frac{D}{\mu_0}(\phi_{f1} + A_{m1}B_{m1}) \quad (19)$$

Therefore, as shown in (19), substituting three equations (14), (15), and (19) into (3) allows that fringing flux $\phi_{f1}$ flowing through air gap of the excitation pole S1 on the path $l_F$ in Fig. 4 is characterized by flux density $B_{m1}$ around air gap of the excitation pole S1 on the main flux path, $l_M$, and (20) is rearranged as in (21).

$$\frac{\phi_{f1}}{\mu A_{f1}} l_{cf} + \frac{\phi_{f1}}{\mu_0 A_{f1}} l_{gf1} + \frac{D}{\mu_0}(\phi_{f1} + A_{m1}B_{m1}) l_{gf2} = N_p \cdot I_p \quad (20)$$

$$\phi_{f1} = \frac{N_p \cdot I_p}{E} - \frac{DA_{m1}l_{gf2}}{\mu_0 E} B_{m1} \quad (21)$$

where

$$E = \frac{l_{cf}}{\mu A_{f1}} + \frac{l_{gf1}}{\mu_0 A_{f1}} + \frac{Dl_{gf2}}{\mu_0} \quad (22)$$

The combination of two equations, (21) and (12), is written as

$$H_{cm} l_{cm} = N_p I_p - \frac{Cl_{m2}}{\mu_0}\left(\frac{N_p I_p}{E} - \frac{DA_{m1}l_{gf2}}{\mu_0 E} B_{m1}\right) - \frac{1}{\mu_0}(l_{gm1} + CA_{m1}l_{gm2}) B_{m1} \quad (23)$$

$$\therefore H_{cm} = F\frac{N_p I_p}{l_{cm}} - \frac{B_{m1}}{\mu_0 l_{cm}} l_{gm} \quad (24)$$

where

$$F = 1 - \frac{Cl_{gm2}}{\mu_0 E} \quad (25)$$

$$l_{gm} = l_{gm1} + CA_{m1}l_{gm2} - \frac{Cl_{gm2}DA_{m1}l_{gf2}}{\mu_0 E} \quad (26)$$

It is noted in (24) that the magnetic field intensity ($H_{cm}$) of iron in case of main flux is expressed by the variation of the air-gap flux density ($B_{m1}$) around the excitation pole S1 in conjunction with dimensional change and material nonlinearity in variables, F and $l_{gm}$. Since there are two unknowns, $H_{cm}$ and $B_{m1}$, in (24), another equation is necessary to find a unique solution. Realizing that $\phi_{m1}$ in Fig. 5 flows through both steel and air gap of the excitation pole S1, $B_{m1}$ is able to also represent flux density in the energized stator pole due to the same cross-sectional area in the steel and air gap. In [8], the behavior of steel is analytically given in terms of magnetic field intensity and flux density by introducing a variable denoting saturated flux density ($B_{sat}$) as written in (27).

$$B_{m1} = \frac{\mu H_{cm}}{1 + \frac{\mu H_{cm}}{B_{sat}}} + \mu_0 H_{cm} \quad (27)$$

By substituting (24) into (27), a single-unknown equation is obtained, and it is rearranged as a quadratic equation for $B_{m1}$ as shown in (28).

$$s_1 B_{m1}^2 + s_2 B_{m1} + s_3 = 0 \quad (28)$$

where

$$s_1 = \frac{\mu l_{gm}}{\mu_0 l_{cm}}\left(1 + \frac{l_{gm}}{l_{cm}}\right) \quad (29)$$

$$s_2 = -B_{sat}\left\{1 + \frac{\mu F N_p I_p}{l_{cm} B_{sat}}\left(1 + \frac{2l_{gm}}{l_{cm}}\right) + \frac{l_{gm}}{l_{cm}}\left(1 + \frac{\mu}{\mu_0}\right)\right\} \quad (30)$$

$$s_3 = B_{sat}\left\{F\frac{N_p I_p}{l_{cm}}(\mu + \mu_0) + \frac{\mu_0 \mu}{B_{sat}}\left(F\frac{N_p I_p}{l_{cm}}\right)^2\right\} \quad (31)$$

After dividing by $s_1$, (28) is simplified to (32) from which the solution of $B_{m1}$ is easily determined to satisfy the given quadratic equation as derived in (35).

$$B_{m1}^2 + \alpha_1 B_{m1} + \alpha_2 = 0 \quad (32)$$

where

$$\alpha_1 = -\frac{B_{sat}}{1 + \frac{l_{gm}}{l_{cm}}}\left\{\frac{\mu_0}{\mu}\left(\frac{l_{cm}}{l_{gm}} + \frac{\mu}{\mu_0} + 1\right) + \frac{\mu_0 F N_p I_p}{l_{gm} B_{sat}}\left(1 + \frac{2l_{gm}}{l_{cm}}\right)\right\} \quad (33)$$

$$\alpha_2 = \frac{s_3}{s_1} = \frac{B_{sat}}{1 + \frac{l_{gm}}{l_{cm}}}\left\{\frac{\mu_0 F N_p I_p}{\mu l_{gm}}(\mu + \mu_0) + \frac{(\mu_0 F N_p I_p)^2}{B_{sat} l_{gm} l_{cm}}\right\} \quad (34)$$

$$B_{m1} = 0.5\left[\frac{B_{sat}}{1 + \frac{l_{gm}}{l_{cm}}}\left\{\frac{\mu_0}{\mu}\left(\frac{l_{cm}}{l_{gm}} + \frac{\mu}{\mu_0} + 1\right) + \frac{\mu_0 F N_p I_p}{l_{gm} B_{sat}}\left(1 + \frac{2l_{gm}}{l_{cm}}\right)\right\}\right] \pm \sqrt{\gamma} \quad (35)$$

where

$$\gamma = \frac{B_{sat}^2}{\left(1 + \frac{l_{gm}}{l_{cm}}\right)}\left\{\frac{\mu_0}{\mu_0}\left(\frac{l_{cm}}{l_{gm}} + \frac{\mu_0}{\mu_0} + 1\right) + \frac{\mu_0 F N_p I_p}{l_{gm} B_{sat}}\left(1 + \frac{2l_{gm}}{l_{cm}}\right)\right\}^2 \quad (36)$$

Regarding the phase current $I_p$ in (36), the equation is reorganized as a quadratic form as following.

$$\gamma = \delta_2 I_p^2 + \delta_1 I_p^1 + \delta_0 I_p^0 \tag{37}$$

where

$$\delta_2 = \frac{(\mu_0 F N_p)^2}{\left(1+\frac{l_{gm}}{l_{cm}}\right)^2}\frac{1}{l_{gm}^2} \tag{38}$$

$$\delta_1 = \frac{(\mu_0 F N_p)^2}{\left(1+\frac{l_{gm}}{l_{cm}}\right)^2}\frac{1}{l_{gm}^2}\frac{2B_{sat}}{\mu F N_p}\left\{l_{cm}-\left(\frac{\mu}{\mu_0}-1\right)l_{gm}\right\} \tag{39}$$

$$\delta_0 = \frac{B_{sat}^2}{\left(1+\frac{l_{gm}}{l_{cm}}\right)^2}\left(\frac{\mu_0}{\mu}\right)^2\left(\frac{l_{cm}}{l_{gm}}+\frac{\mu}{\mu_0}+1\right)^2 \tag{40}$$

As a result, using equations (35) and (37), two solutions for $B_{m1}$ can be obtained due to positive and negative signs in front of the square root in (35). However, only one solution for $B_{m1}$ having the negative square root is finally chosen by the fact that the flux density $B_{m1}$ has to be zero with no phase current as given in (41).

$$B_{m1} = \frac{0.5}{1+\frac{l_{gm}}{l_{cm}}}\frac{\mu_0 F N}{l_{gm}}\left[\left(1+\frac{2l_{gm}}{l_{cm}}\right)I_p+\frac{B_{sat}l_{m1}}{\mu F N_p} - \sqrt{I_p^2+\frac{2B_{sat}l_{m2}}{\mu F N_p}I_p+\left(\frac{B_{sat}l_{m1}}{\mu F N_p}\right)^2}\right] \tag{41}$$

where

$$\frac{\mu}{\mu_0} = \mu_r \tag{42}$$

$$l_{m1} = l_{cm} + (\mu_r + 1) l_{gm} \tag{43}$$

$$l_{m1} = l_{cm} + (\mu_r + 1) l_{gm} \tag{44}$$

From (41), it is easy to derive the analytical expression of main flux linkage as given by

$$\lambda_{m1}(\theta, I_{ph}) = n_s N_p \phi_{m1} = n_s N_p A_{m1}[B_{m1}]_{I_p \to I_{ph}/n_p} \tag{45}$$

$$\lambda_{m1}(\theta, I_{ph}) = \lambda_0 \frac{r_s \theta}{\left(1+\frac{l_{gm}}{l_{cm}}\right)}\left[\left(1+\frac{2l_{gm}}{l_{cm}}\right)\frac{I_{ph}}{n_p}+\frac{B_{sat}l_{m1}}{\mu F N_p} - \sqrt{\left(\frac{I_{ph}}{n_p}\right)^2+\frac{2B_{sat}I_{m2}}{\mu F N_p}\frac{I_{ph}}{n_p}+\left(\frac{B_{sat}l_{m1}}{\mu F N_p}\right)^2}\right] \tag{46}$$

where

$$\lambda_0 = 0.5 n_s \mu_0 F N_p^2 l \tag{47}$$

where $r_s$ and $\theta$ are stator bore radius and overlap angle between stator and rotor poles on the main flux path, respectively. $n_p$, $n_s$, $l$ l, and $I_{ph}$ are number of parallel windings per phase, number of series windings per phase, stack length of the motor, and phase current, respectively.

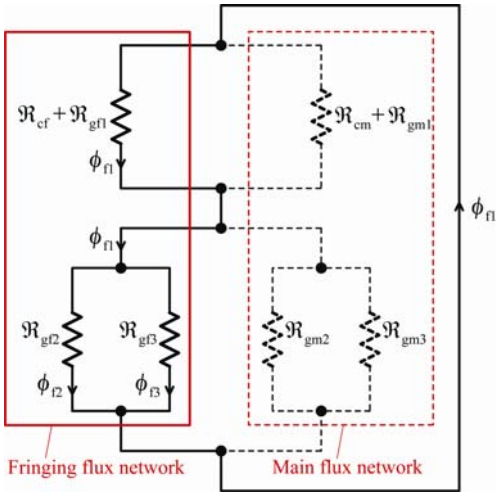


**Fig. 6.** (Color online) Reluctance network of single-body E-core SRM at the unaligned position.

### 3.3. Calculation of fringing flux linkage

In case of no overlap between stator excitation and rotor poles, there is no main flux path as shown in Fig. 6. Hence, all equations from (48) to (51) are the same as those derived in the previous section.

$$H_{cf} \cdot l_{cf} + H_{gf1} \cdot l_{gf1} + H_{gf2} \cdot l_{gf2} = N_p \cdot I_p \tag{48}$$

$$B_{f1} = \mu H_{cf} = \mu_0 H_{gf1} \tag{49}$$

$$H_{cf} = \frac{B_{f1}}{\mu} \tag{50}$$

$$H_{gf1} = \frac{B_{f1}}{\mu_0} \tag{51}$$

Flux density in air gap of the common pole, C4, in Fig. 4 is characterized only by $\phi_{f1}$, and the main flux does not affect the flux density ($B_{f2}$) in this case.

$$B_{f2} = \mu_0 H_{gf2} = \frac{\phi_{f2}}{A_{f2}} = \frac{1}{A_{f2}}\left(\phi_1 \frac{\Re_{gf2}}{\Re_{gf2}+\Re_{gf3}}\right) \tag{52}$$

From (51), hence, $H_{gf2}$ becomes

$$H_{gf2} = \frac{A_{f1}}{A_{f2}}\frac{B_{f1}}{\mu_0} G \tag{53}$$

where

$$G = \frac{l_{gf3} A_{f2}}{l_{gf2} A_{f3} + l_{fg3} A_{f2}} \tag{54}$$

By substituting (51) and (53) into (48), $H_{cf}$ is given by

$$H_{cf} = \frac{N_p I_p}{l_{cf}} - \frac{l_{gf}}{\mu_0 l_{cf}} B_{f1} \tag{55}$$

where

$$l_{gf} = l_{gf1} + G\frac{A_{f1}}{A_{f2}} l_{gf2} \tag{56}$$

Using (50) and (55), flux density $B_{f1}$ is derived as

$$B_{f1} = \left(\mu \frac{N_p I_p}{l_{cf}}\right) \Big/ \left(1 + \frac{\mu l_{gf}}{\mu_0 l_{cf}}\right) \tag{57}$$

From the fringing flux density ($B_{f1}$) in air gap around a stator excitation pole, the unaligned inductance ($L_{po}$) as a key term can be calculated as

$$L_{po} = \frac{n_s N_p}{n_p I_p} B_{f1,po} A_{f1,po} \tag{58}$$

where

$$B_{f1,po} = \left(\mu_{po} \frac{N_p I_p}{l_{cf}}\right) \Big/ \left(1 + \frac{\mu_{po} l_{gf0}}{\mu_0 l_{cf}}\right) \tag{59}$$

$$A_{f1,po} = w_{sp} \cdot l \tag{60}$$

where $B_{f1,po}$, $A_{f1,po}$, $\mu_{po}$, and $l_{gf0}$ are $B_{f1}$, $A_{f1}$, $\mu$, and $l_{gf}$ at the beginning of overlap between stator excitation and rotor poles, respectively

Using (58), as a result, the air-gap length of fringing flux at the beginning of overlap position is analytically derived by

$$l_{gf0} = \frac{n_s}{n_p} \frac{\mu_0 \cdot N_p^2 \cdot w_{sp} \cdot l}{L_{po}} - \frac{\mu_0}{\mu_{po}} l_{cf} \tag{61}$$

The air-gap length of fringing flux is assumed to be a function of rotor position. The length becomes $l_{gf0}$ as its maximum at the beginning of overlap, and its minimum is found as $l_{fg,a}$ derived from (56) as written in (62). Also, it is assumed that the air gap varies linearly in between.

$$l_{gf,a} = l_{gf1,a} + G_a \frac{A_{f1,a}}{A_{f2,a}} l_{gf2,a} \tag{62}$$

where $l_{gf,a}$, $l_{gf1,a}$, $G_a$, $A_{f1,a}$, $A_{f2,a}$, and $l_{gf,a}$ are $l_{gf}$, $l_{gf1}$, G, $A_{f1}$, $A_{f2}$, and $l_{gf2}$ at the fully aligned rotor position, respectively.

Therefore, the sum of main flux density ($B_{m1}$) in (41) and fringing flux density ($B_{f1}$) in (57) leads to total flux linkage of phase windings for the single-body E-core SRM.

## 4. Verification of Analytical Flux Linkage

The analytical model of phase flux linkage is developed by means of separation of main and fringing flux paths at a rotor position in which a set of stator excitation poles experiences partial overlap with rotor poles, and hence, the model allows flux linkage to be calculated with respect to rotor position at various levels of phase current. Flux linkage of the single-body E-core SRM designed in the previous chapters is mathematically obtained and

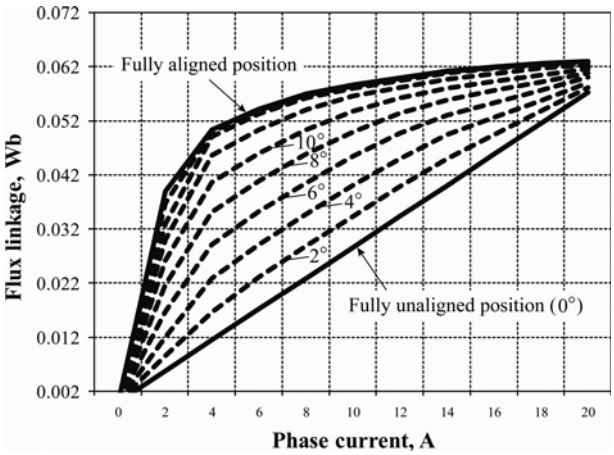


**Fig. 7.** Analytical flux linkage of single-body E-core SRM.

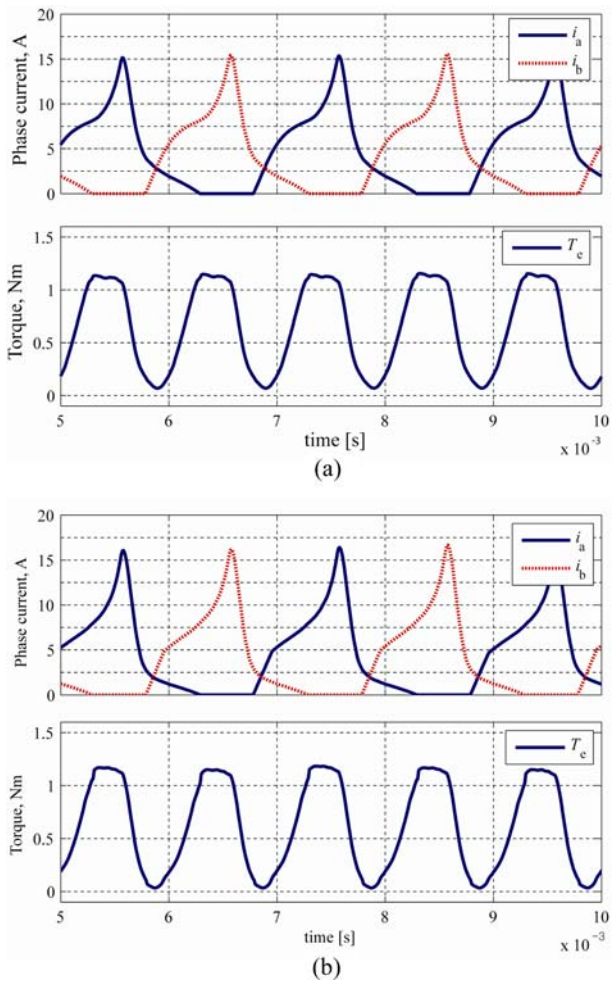


**Fig. 8.** (Color online) Phase current and torque prediction in E-core SRM @ 3000 rpm, (a) FEA, (b) Reluctance network.

plotted from the unaligned to aligned rotor position in steps of 2° angle as given in Fig. 7.

To verify the analytical flux linkage, dynamic simulation is conducted under single pulse operation at 3000 rpm, and the results for flux linkage are compared with those given from FEA and plotted in Fig. 8. The average torque is 0.648 Nm for the FEA flux linkages and 0.623 Nm for analytical flux linkage. Since the difference is approximately 4%, this analytical flux linkage can be used for the design of a motor within a reasonable error.

## 5. Conclusion

The accurate prediction of flux linkage with respect to rotor position makes a significant contribution to designing an SRM and its analytical approach is not straightforward due to nonlinear flux distribution. FEA and curve-fitting tool are not suitable for a simple design procedure because the FEA necessitates a large amount of time in both modeling and solving with complexity for every motor design, and the curve-fitting requires the data of flux linkage from either an experimental test or an FEA simulation. Also, MEC technique becomes one of the candidates for predicting flux linkage, but it still requires a large amount of numerical derivation representing lots of complex permeances. In this paper, flux linkage at aligned and unaligned rotor positions is estimated by means of a simple reluctance network, and the proposed approach is analytically verified in terms of accuracy compared to FEA simulation. To verify the analytical flux linkage, dynamic simulation is conducted under single pulse operation at 3000 rpm, and the results for flux linkage are compared with those given from FEA. The average torque is 0.648 Nm for the FEA flux linkages and 0.623 Nm for analytical flux linkage. Since the difference is approximately 4%, this analytical flux linkage can be used for the design of a motor within a reasonable error.

## Acknowledgment

This research was supported by Kyungsung University Research Grants in 2013.

## References

[1] R. Krishnan, “Switched Reluctance Motor Drives”, CRC (2001).
[2] D. A. Torrey and J. H. Lang, Proc. Inst. Elect. Eng., pt. B **137**, 314 (1990).
[3] T. J. E. Miller and McGilp, Proc. Inst. Elect. Eng., pt. B **137**, 337 (1990).
[4] D. A. Torrey, Electric Machines Power Syst. **24**, 199 (1996).
[5] M. Stiebler and K. Liu, IEEE Trans. Energy Conversion **14**, 1100 (1999).
[6] James M. Kokernak and David A. Torrey, IEEE Trans. Magn. **36**, 500 (2000).
[7] Cheewoo Lee and R. Krishnan, IEEE Trans. Ind. Appl. **45**, 1804 (2009).
[8] Arthur V. Radun, IEEE Trans. Ind. Appl. **31**, 1079 (1995).